Three-Dimensional Elastic Analysis of a Composite Double Cantilever Beam Specimen

I. S. Raju* and K. N. Shivakumar*
Analytical Services and Materials, Inc., Hampton, Virginia
and
J. H. Crews Jr.†
NASA Langley Research Center, Hampton, Virginia

A three-dimensional elastic analysis of a 24-ply cocured double cantilever beam specimen is presented. Both the graphite adherends and the resin-rich layer were modeled using 20-noded, parabolic isoparametric finite elements. Stresses and the strain energy release rate G along the delamination front (width direction) were studied; G was calculated from Irwin's virtual crack closure technique and from the crack opening displacement method. Stresses were nearly constant over 75% of the interior width and decreased significantly at the outer free surfaces of the specimen. The strain energy release rates were constant over the interior 50% of the delamination front. At the midplane, the strain energy release rate was about 8% higher than the corresponding two-dimensional plane strain value. At the free surface, the strain energy release rate was considerably smaller than the plane strain value. This is believed to be due to the free surface effect that exists where the delamination meets the surface edge. The von Mises and a modified von Mises yield criterion, which included the hydrostatic stress effect, were used with the elastic stresses to estimate the yield zone in the resin-rich layer. The yield-zone lengths were considerably larger when the hydrostatic tension stress was included in the yield criterion than when the hydrostatic stress was neglected (as in the von Mises criterion).

Nomenclature

a	= delamination length, m
E_{xx},E_{yy},E_{zz}	= Young's modulus of the adherend in the x-, y-, and z- directions, respectively, Pa
E_r	= Young's modulus of the resin, Pa
G	= total strain energy release rate, N/m
G_{xy},G_{xz},G_{yz}	= shear modulus of the adherend material, Pa
G_r	= resin shear modulus, Pa
h	= thickness of each adherend, m
P	= applied load per unit width, N/m
t	= half thickness of the resin layer, m
u,v,w	= Cartesian displacements in x-, y-, and z- directions, respectively, m
W	= width of the specimen, m
x,y,z	= Cartesian coordinates, m
$\{\sigma\}$	= Cartesian stresses, σ_x, σ_y, σ_z, σ_{xy}, σ_{yz}, σ_{zx}, Pa
σ_m	= hydrostatic stress, Pa
σ_{ys}	= yield stress of the resin, Pa
τ_{oct}	= octahedral shear stress, Pa
$\nu_{xy},\nu_{xz},\nu_{yz}$	= Poisson's ratio of the adherend
ν_r	= Poisson's ratio of the resin
Δ	= size of the delamination tip element

Subscripts

r	= resin
$p\varepsilon$	= plane strain

Presented as Paper 87-0864CP at the 28th AIAA/ASME/AHS/ASEE Structures, Structural Dynamics and Materials Conference, Monterey, CA, April 6–8, 1987; received May 13, 1987; revision received Nov. 17, 1987.

*Senior Scientist.
†Senior Scientist, Materials Division.

Introduction

DOUBLE cantilever beam (DCB) specimens (Fig. 1) are widely used to measure the delamination fracture toughness of composite laminates. These specimens characterize the mode I resin toughness in the presence of adherend constraints. Detailed two-dimensional finite-element analyses of the specimen were presented in Refs. 1 and 2. In Ref. 2, the specimen was idealized as two orthotropic adherends with a resin-rich (isotropic) interface. Stress distributions ahead of the delamination and stress-intensity factors for various specimen configurations were examined. However, to examine the variation of stresses across the specimen width, a three-dimensional analysis is needed. No such analysis has been reported in the literature. The first objective of this paper is to compute three-dimensional stresses ahead of the delamination front in a DCB specimen. A three-dimensional finite-element analysis was conducted for a graphite/epoxy specimen with dimensions and material properties similar to those used in the two-dimensional analysis in Ref. 2.

The interlaminar fracture toughness of a DCB specimen usually is expressed in terms of G, the strain energy release rate, for delamination growth. Until recently, only two-dimensional analyses were used to calculate the G values. These analyses give only an average value across the width of the specimen. The distribution of G across the specimen width requires a three-dimensional analysis. Such an analysis would also identify which of the two-dimensional analyses (plane stress or plane strain) provides the better approximation of the G distribution. Thus, the second objective of this paper is to present a three-dimensional strain energy release rate analysis of the DCB specimen.

Experimental data have shown that the hydrostatic tension (dilatational) stress component of the applied stress tensor influences yielding of some thermoplastic resins.[3] This contrasts with metal behavior, where yielding is usually assumed to depend solely on the deviatoric (octahedral shear) stress component. Near a delamination, the interlaminar stress state may have a large hydrostatic tension component because of the adherend restraints on the interface deformations. This may influence interlaminar fracture toughness in some resin-based laminates. The third objective of this paper is to analyze the

hydrostatic stress component near the delamination front and estimate its effect on yielding of thermoplastics.

Analysis

In this section, first, the DCB specimen configuration and loading are described. Next, the three-dimensional finite-element modeling of the specimen is presented. Last, the methods used to compute the strain energy release rate are presented.

Specimen Configuration

Figure 1 shows the DCB specimen configuration and loading. The specimen consists of two cocured adherends with a thin resin layer of thickness $2t$. Each adherend represents a 12-ply unidirectional T300/5208 graphite/epoxy laminate of thickness h. A delamination is located in the thin resin interface layer. The specimen dimensions and elastic properties of the unidirectional laminate[4] (fibers in the x-direction) are as follows: delamination length, $a = 50.8$ mm (2 in.); specimen width, $W = 25.4$ mm (1 in.); adherend thickness, $h = 1.65$ mm (0.0648 in.); resin thickness, $2t = 0.01$ mm (4×10^{-4} in.).

The specimen is loaded, as shown in Fig. 1, by imposing uniform displacements in the y-direction. The load per unit width required for the uniform v-displacement is denoted as P. Unless otherwise specified, the results in this paper correspond to $P = 1$ N/m. Because of the symmetric configuration and loading, pure mode I deformations occur in the specimen.

Finite-Element Model

Because the specimen is symmetric about the $y = 0$ and $z = 0$ planes, only one-quarter of the specimen was modeled. Figure 2 shows a typical three-dimensional finite-element model. In this model, 20-noded isoparametric parabolic elements were used everywhere except along the delamination front where collapsed quarter-point singularity elements were used.[5,6] Figure 2 shows the details of the modeling at the delamination front on any z = constant plane.

The finite-element model was developed by modeling the $z = 0$ plane and translating that plane in the z-direction. The model on the $z = 0$ plane is the same model as that used in Ref. 2. The two-dimensional model in Ref. 2 was developed by

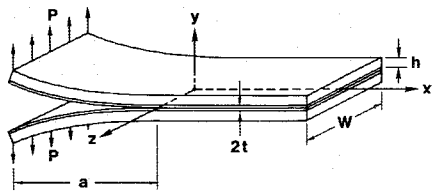

Fig. 1 Configuration of a double cantilever beam.

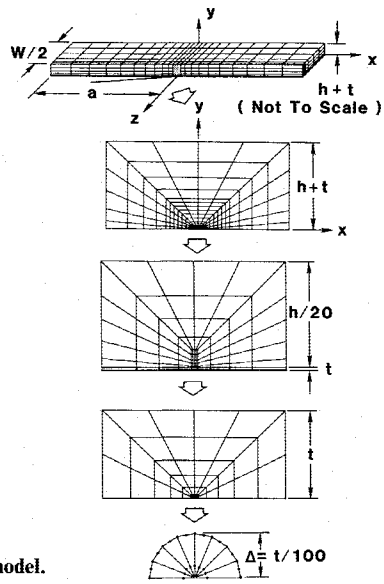

Fig. 2 Finite-element model.

conducting a convergence study on the strain energy release rates. The two-dimensional model gave strain energy release rates within 1% of the classical and other finite-element solutions. Therefore, the model on each z = constant plane was judged to be adequate, and only refinements in the width direction are needed to establish an accurate three-dimensional model. To this end, three models with four, five, and six layers were developed. The four-layer model had four equal layers across the width. The five-layer model was developed from the four-layer model by dividing the layer nearest to the free surface (at $z = W/2$) into two equal layers. Similarly, the six-layer model was obtained from the five-layer model by again subdividing the free surface layer into two equal layers. The six-layer model had 2808 elements and 13,567 nodes with 40,707 degrees of freedom. The thickness-to-width aspect ratios of the elements at the intersection of the delamination front and the free surface of the specimen are very large. However, this did not cause a singularity of the stiffness matrix or numerical roundoff problems in the solution. Also, no convergence difficulties were encountered for strain energy release rates, displacements, or stresses. The convergence of displacements, stresses, and strain energy release rates is discussed in a later section.

Computation of Strain Energy Release Rates

Two methods were used to calculate the strain energy release rates: the crack opening displacement (COD) method and Irwin's virtual crack closure technique (VCCT).

Crack Opening Displacement Method

The COD method uses the crack opening displacements at the quarter-point nodes and at the corner nodes to determine the stress-intensity factors and strain energy release rates.[5-7] Because this method is based on the near-field two-dimensional solution, the method requires an assumption of either plane stress or plane strain. Plane strain is usually assumed (see Ref. 7). If v_q and v_Δ are the relative opening displacements at the quarter-point and the corner nodes, respectively (see Fig. 3a), then assuming plane strain, the stress-intensity factor is given by[5,7]

$$K = \frac{E_r v}{4(1-\nu_r^2)}\left(\frac{2\pi}{\delta}\right)^{\frac{1}{2}} \tag{1}$$

where $v = v_q$ and $\delta = \Delta/4$ for quarter-point nodes, and $v = v_\Delta$ and $\delta = \Delta$ for corner nodes.

Table 1 Material properties for resin and adherend

	Resin[4]	Adherend[4]
E_{xx}	3.4 GPa	134.4 GPa
E_{yy}	3.4 GPa	13.0 GPa
ν_{xy}	0.3	0.34
ν_{yz}	0.3	0.35
G_{xy}	1.3 GPa	6.4 GPa
G_{yz}	1.3 GPa	4.8 GPa

$E_{zz} = E_{yy}$, $\nu_{xz} = \nu_{xy}$, and $G_{xz} = G_{xy}$

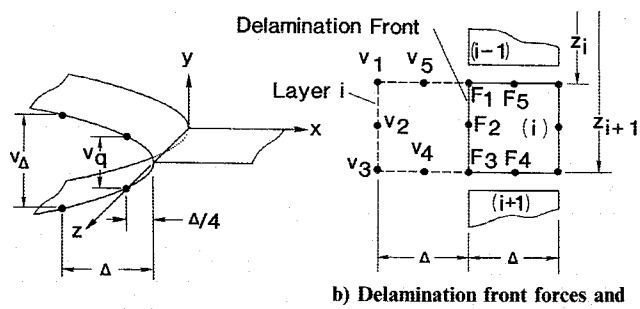

a) COD at singularity element codes

b) Delamination front forces and opening displacements in the ith layer ($y = 0$ plane)

Fig. 3 Computation of strain energy release rates.

In Eq. (1), either the quarter-point or the corner node displacements are used. Freese and Tracey[8] suggested a third method that uses a combination of the quarter-point and the corner node displacements as $v = 4v_q - v_\Delta$ and $\delta = \Delta$ in Eq. (1) to calculate the stress-intensity factor. All three methods give nearly identical stress-intensity factors under plane strain conditions. The strain energy release rates are obtained from the stress-intensity factor as

$$G = K^2(1 - \nu_r^2)/E_r \tag{2}$$

Equations (1) and (2) were used at every z = constant plane along the delamination surface where the nodal displacements are available to obtain the strain energy release rates. As previously mentioned, the COD method requires an assumption of either plane stress or plane strain. The strain energy release rates obtained by either assumption differ by a factor of $(1 - \nu_r^2)$.

Virtual Crack Closure Technique

The VCCT uses the stresses ahead of the delamination front ($x > 0$) and the displacements behind the front ($x < 0$). This method does not require an assumption of either plane stress or plane strain. A simple formula for calculating the strain energy release rates in two-dimensional analyses was given by Rybicki and Kanninen.[9] This formula for four-noded elements was developed using the VCCT and uses the forces at the crack tip and the relative displacements of the crack faces behind the crack tip. Similar formulas were developed for quarter-point singularity and higher-order nonsingular elements by Raju.[10] Extension of these formulas for three-dimensional analyses with singularity elements requires further study. However, extension of these formulas to three-dimensional nonsingular elements is straightforward. Therefore, another six-layer model that uses collapsed 20-noded nonsingular elements was developed. This new model was obtained by moving the quarter-point nodes in the previous model to midside positions. The strain energy release rates were calculated from the work required to close the delamination by one element length Δ (see Fig. 3b) as

$$G = \sum_{j=1}^{5} (F_j v_j)/[\Delta(z_{i+1} - z_i)] \tag{3}$$

where F_j are the forces in the y-direction at node j calculated from all of the elements surrounding the delamination front in the ith layer of the model. Note that the forces F_4 and F_5 are computed from only one element ahead of the delamination front in the ith layer. Equation (3) gives the average value of the strain energy release rate for the ith layer and is interpreted as the G-value at the center of that layer. When applied to each layer in the finite-element model, Eq. (3) gives the distribution of the strain energy release rate across the width of the specimen.

Results and Discussion

Convergence Study

As mentioned earlier, the two-dimensional finite-element model[2] used in the $z = 0$ plane gave accurate stress distributions and G values. Therefore, the convergence of the finite-element solution was studied as the model was refined in the width direction. The convergence of the delamination opening displacements v is presented here. The convergence of the strain energy release rate will be presented later in this paper.

Figure 4 presents the delamination opening displacement distribution near the delamination front obtained with the four-, five-, and six-layer models. At $z = 0$, the v-displacement profiles obtained with the three idealizations were virtually identical for all three models. At the free surface ($z = W/2$), smaller v-displacements were obtained with increasing refinement. However, the differences between the five- and six-layer models are small compared to those between the four- and five-layer models. Thus, the six-layer model was considered to have adequate refinement across the width and, hence, was used in the remainder of the analyses.

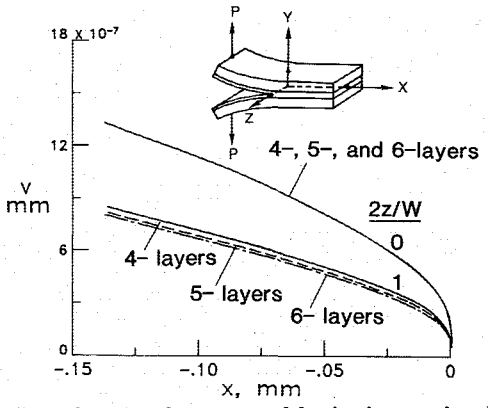

Fig. 4 Effect of mesh refinement on delamination opening displacements.

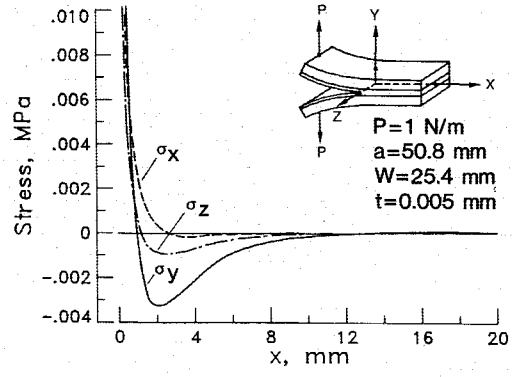

Fig. 5 Normal stress distribution ahead of delamination front, $y = z = 0$.

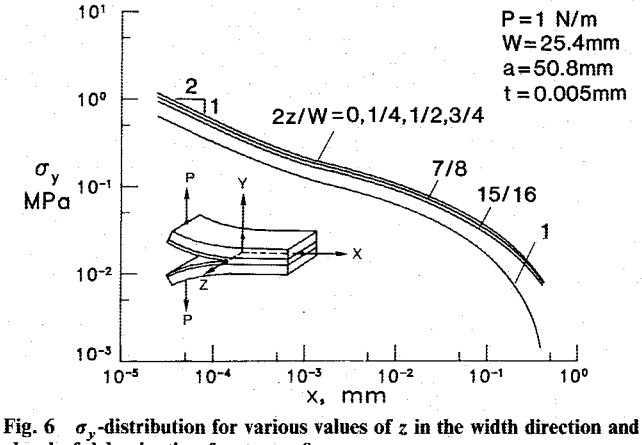

Fig. 6 σ_y-distribution for various values of z in the width direction and ahead of delamination front, $y = 0$.

Normal Stress Distributions

Figure 5 presents the normal stress σ_x, σ_y, and σ_z distributions on the midplane ($z = 0$) ahead of the delamination front. Very near the delamination tip, the stresses show a steep gradient because of the square-root singularity. The dominant stress for this opening mode case is the σ_y normal stress. This stress shows a sign reversal at about 1 mm (a distance of about 100 resin thicknesses) from the delamination tip and decreases to near-zero at distances greater than about 15 mm. The stresses σ_x and σ_z diminish to near-zero values much nearer to the delamination tip. Because the region of severe stress gradient is very small, the σ_y stresses are shown in Fig. 6 on a log-log plot

for various $2z/W$ values. The σ_y stress distributions have a linear portion with a slope of -0.5 for values of x less than about 0.001 mm, reflecting the square-root singularity. For larger x values, the stress distributions deviate from a linear relation and have a "hump," as discussed for the two-dimensional case in Ref. 2. All stations across the delamination front for all $2z/W$ values show this behavior.

The σ_y stress is largest at the midplane and is progressively smaller for larger values of $2z/W$. The reduction is most pronounced near the free surface (compare values for $2z/W = 1$ and 15/16 curves). The σ_x and σ_z stresses have similar trends and, hence, are not shown. Very near the delamination front ($x \leq 0.01$ mm), the σ_x stresses are nearly equal to σ_y stresses, and the σ_z stresses are only slightly lower. The mean stress σ_m, therefore, has a magnitude nearly as high as the normal stress.

Constraint Ahead of the Delamination Front

To study the state of stress ahead of the delamination front, the constraint factor $\sigma_z/[\nu_r(\sigma_x + \sigma_y)]$ was computed. If plane strain conditions exist, the constraint factor equals unity. On the other hand, if plane stress conditions exist, the factor will be zero. Figure 7 presents the constraint factor as a function of $2z/W$ at various locations x ahead of the delamination front. In the interior of the specimen (small $2z/W$ values), plane strain conditions exist for all x values. Very close to the delamination front (small x values), plane strain conditions exist all across the specimen width. However, ahead of the delamination tip, plane strain conditions are present only in the specimen interior. For example, when $x = 0.0001$ mm, plane strain conditions exist for most of the width of the specimen, whereas for $x = 0.4$ mm, the plane strain zone covers only about 75% of the specimen width. At $x = 0.4$ mm and at the free surface ($2z/W = 1$), the constraint factor is about 0.2, indicating that the stress state is closer to plane stress than plane strain.

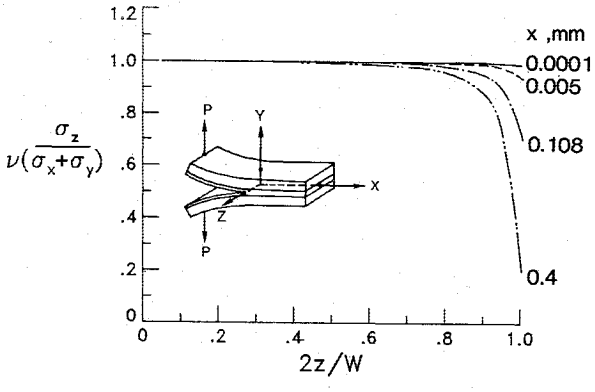

Fig. 7 Constraint factor for various values of x ahead of delamination front, $y = 0$.

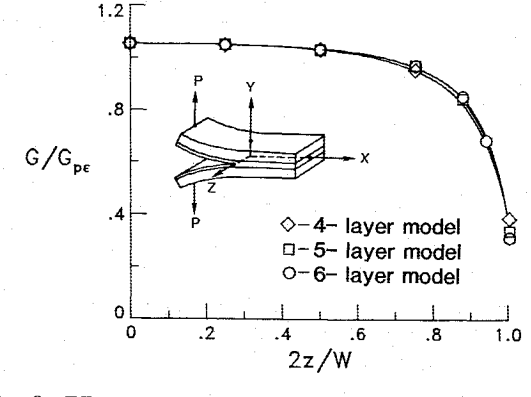

Fig. 8 Effect on G-distribution of mesh refinement in the width direction.

Strain Energy Release Rates

As mentioned earlier, two different procedures were used to calculate the strain energy release rates. In the first procedure, the three finite-element models with quarter-point singularity elements were used, and the strain energy release rates were calculated using the COD method. In the second procedure, the six-layer model with nonsingular elements was used with the VCCT.

In the first procedure, plane strain conditions were assumed all across the delamination front. For a 1 N/m load, the corresponding two-dimensional value of the strain energy release rate $G_{p\varepsilon}$ was calculated to be 0.57 N/m. Table 2 and Fig. 8 present the strain energy release rates across the delamination front for the three idealizations using the COD method. The $G_{p\varepsilon}$ value was used to normalize these computed three-dimensional results.

For $0 \leq 2z/W \leq 0.75$, the differences between the five- and six-layer models are very small, showing good convergence. At $2z/W = 0.75$, the difference between the four- and the five-layer models is about 2%, whereas the difference between the five- and six-layer models is less than 0.1%. The differences between the models are larger as $2z/W$ becomes larger. The largest difference between the five- and six-layer models is at the free surface and is about 9%. These results confirm the earlier conclusion that the six-layer model has sufficient refinement in the width direction.

As shown in Fig. 8, at the free surface all three models show a significant drop in the strain energy release rate. Also, the strain energy release rates at the free surface do not appear to converge as they did for lower values of $2z/W$. This behavior will be further investigated by comparing these values with those obtained using the VCCT.

The strain energy release rate distribution across the delamination front using the VCCT and the nonsingular element model is shown in Fig. 9. The results obtained with the COD method and the six-layer model from Table 2 are also included in this figure. The strain energy release rates are constant over 50% of the delamination front. At the midplane, the G value from VCCT is about 8% higher than the plane strain value, whereas that from the COD method is about 5% higher. Similar behavior is observed all across the delamination front, with the VCCT consistently giving values that are 3% higher than the COD method. Also, the average value of the strain energy release rates across the delamination front (hereafter referred to as the global average) is

$$G_{av} = \frac{1}{W}\int_0^W G(z)\,dz \tag{4}$$

The G_{av} value was computed by numerical integration from the distributions presented in Fig. 9. The global average obtained with the VCCT was about 1% higher than the two-dimensional plane strain value, whereas that from the COD is about 2% lower. Thus, the two-dimensional plane strain value gives a very good estimate of the global average value of the strain energy release rate in a DCB specimen and can be used confidently.

Table 2 Normalized strain energy release rates $G/G_{p\varepsilon}$ using COD method ($G_{p\varepsilon} = 0.57 \times 10^{-4}$ N/m)

	Layers in the model		
$2z/W$	4	5	6
0.0	1.0475	1.0475	1.0475
0.25	1.0435	1.0444	1.0444
0.50	1.0267	1.0279	1.0282
0.75	0.9514	0.9658	0.9667
0.875	—	0.8404	0.8505
0.9375	—	—	0.6823
1.0	0.3863	0.3381	0.3118

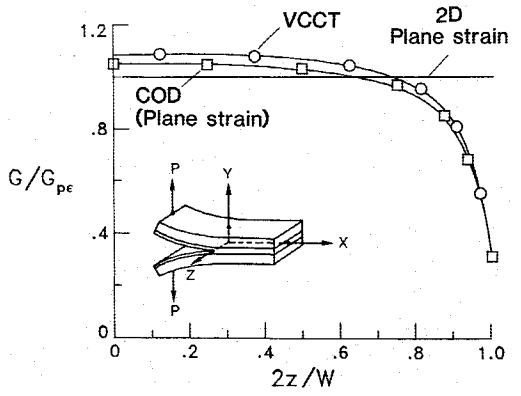

Fig. 9 Distribution of strain energy release rate along delamination front.

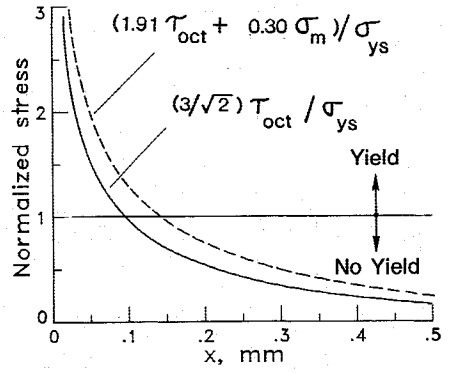

Fig. 10 Effect of hydrostatic stress on yielding in the resin layer, $y = z = 0$.

Close to the free surface ($2z/W \geq 0.75$), the G values by either method show a significant drop when compared to the two-dimensional plane strain solution. This is believed to be due to the "free surface effect" when a delamination or a crack meets a free surface. Considerable work on this free surface effect for through-the-thickness and surface cracks in metallic solids has been reported in the literature. Hartranft and Sih[11] hypothesized that when a crack meets a free surface, there exists a boundary layer in which the stress-intensity factor (and, hence, strain energy release rate) shows a drop, and at the free surface the stress-intensity factor is zero. Later, Benthem[12] showed that at the intersection of the crack front and a free surface, the singularity does not have the classical square-root power but is a function of the material Poisson's ratio. The numerical investigations, however, show that free surface stress-intensity factors drop significantly but never reach a zero value unless arbitrarily forced to zero in the finite-element solution.[7,13–15] Thus, even for isotropic materials, the issue of the free surface is not resolved. Very little work on the free surface effect has been done for cracks or delaminations in orthotropic materials and, in particular, for the DCB specimen. The present solutions using the COD and the VCCT methods are consistent with the other current numerical investigations for the metallic cases and, hence, are considered to be accurate away from the boundary-layer region.

Estimation of Yield Zones

Yielding in metals is generally defined by the von Mises yield criterion. This criterion is based on the distortional energy and neglects the hydrostatic stress component. However, yielding of polymers has been shown in the literature to depend on the hydrostatic component.[3,16–19] A modified von Mises criterion that includes the hydrostatic component was suggested in Ref. 17. This modified criterion is presented in the Appendix and is evaluated using results from the literature for several thermoplastic resins.

Although the present elastic analysis was conducted for a thermoset resin (epoxy) composite DCB, the computed stresses are also believed to be generally applicable to thermoplastic resin composites. For this reason, the computed stresses were used with yield criteria for thermoplastics to estimate the extent of interlaminar yielding ahead of the delamination front. The von Mises and the modified von Mises criteria were used to estimate the yield-zone lengths across the delamination front. The specimen was loaded so that G_{av} was equal to $G_{Ic} = 368$ N/m for the resin material.[2]

The von Mises criterion can be written in terms of the octahedral shear stress as $3\tau_{oct}/(\sqrt{2}\sigma_{ys}) = 1$. Similarly, the modified von Mises criterion can be written as $(1.908\,\tau_{oct} + 0.298\,\sigma_m)/\sigma_{ys} = 1$, where the σ_m is the hydrostatic stress component. Figure 10 presents the normalized stress for both yield criteria as a function of the distance x ahead of the delamination front at the midplane ($z = 0$). All points with normalized stresses equal to or greater than the horizontal line at unity correspond to yielding. All points below this line remain elastic. (No attempt was made to redistribute the stresses carried in the yield zone.) The von Mises criterion predicts an estimated yield-zone length of about 0.09 mm, whereas the modified criterion predicts a larger value of about 0.14 mm. The effect of the hydrostatic component, therefore, increases the estimated yield-zone length by about 50% at the specimen midplane. The significant hydrostatic stress levels ahead of the delamination are caused by the adherend constraint on the local resin deformations.

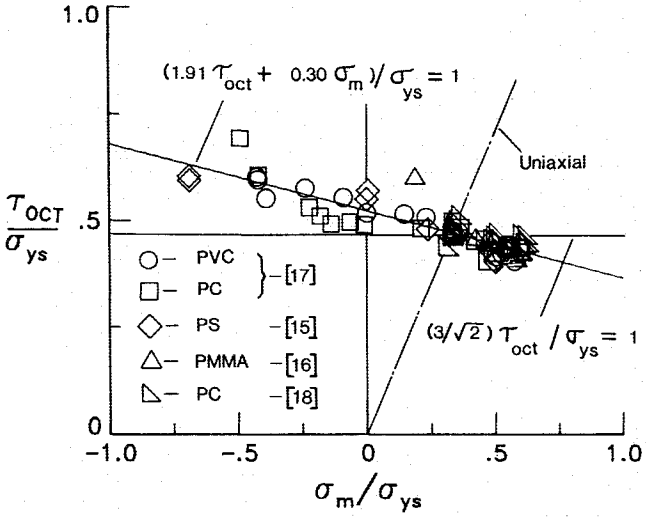

Fig. 11 Effect of hydrostatic stress on yielding of polymeric materials.

Note that the yield-zone length estimate is based on elastic stresses ahead of the delamination front. This estimate is similar to Irwin's estimate for yielding at a crack tip.[20] Because of yielding, there will be stress redistribution that will elongate the yield zones. Thus, the actual yield-zone lengths will be larger than the present estimates from Fig. 10. These estimates should be interpreted as qualitative and are presented here only to show the general effect of hydrostatic stress on yielding near a DCB delamination front. A three-dimensional elastoplastic analysis is needed to quantitatively study the yield zones across the delamination front. The present study shows that such an analysis should account for the effect of the hydrostatic stresses on the inelastic resin response.

Concluding Remarks

An elastic stress analysis of a composite double cantilever beam (DCB) specimen was studied by a three-dimensional finite-element analysis. The strain energy release rates for delamination growth were computed by the crack opening dis-

placement (COD) method and by Irwin's virtual crack closure technique (VCCT). Yield-zone lengths were estimated by two methods: the von Mises yield criterion and a modified von Mises yield criterion that accounts for the hydrostatic stress component. Based on the present study, the following conclusions were drawn.

A plane strain stress state was recovered across 75% of the specimen width. The 25% of the width of the specimen near the free surface was neither in the plane strain nor the plane stress state.

The VCCT and the COD method (assuming plane strain) produced accurate strain energy release rate distributions across the delamination front. The maximum difference between these two methods was about 3%. However, the COD method requires an assumption of the stress state, whereas the VCCT does not. The average of the strain energy release rate distribution, by either VCCT or COD methods, agreed extremely well with the two-dimensional plane strain strain-energy release rate. This suggests that the plane strain value of the strain energy release rate can be confidently used for the DCB specimen.

The strain energy release rates were constant over the interior 50% of the delamination front. At the midplane, the strain energy release rate was about 8% higher than the corresponding two-dimensional plane strain value. At the free surface, the strain energy release rate is considerably smaller than the plane strain value. This may be due to the free surface effect that exists where the delamination meets the surface edge.

The yield-zone lengths, estimated using the elastic stress state, are considerably larger when the hydrostatic tension stress is included in the yield criterion, compared to when it is neglected. Further studies using three-dimensional elastoplastic analyses are needed to quantify the effects of the hydrostatic stress on yielding near delaminations.

Appendix: Yield Criterion Including Hydrostatic Stresses

The yielding of materials under multi-axial stress states is represented by the von Mises yield criterion as

$$\frac{3}{\sqrt{2}}\tau_{oct}/\sigma_{ys} = 1 \qquad \text{(A1)}$$

where τ_{oct} is the octahedral shear stress, and σ_{ys} is the uniaxial yield stress in tension. Equation (A1) was developed based on a distortional energy analysis and assumes that the hydrostatic stress has no influence on yielding. For metallic materials, this appears to be reasonably accurate. However, for polymeric materials, yielding is sensitive to the hydrostatic stress.[3,16–19] A hydrostatic compression stress appears to increase the resistance to yielding, whereas a hydrostatic tensile stress decreases the resistance. Sternstein and Ongchin[17] suggested a modification to Eq. (A1), which is similar to that suggested by Drucker-Prager, to include the effect of the hydrostatic stress. The modified equation is

$$(a_1\tau_{oct} + a_2\sigma_m)/\sigma_{ys} = 1 \qquad \text{(A2)}$$

This equation is referred to herein as the modified von Mises criterion. The constants a_1 and a_2 were obtained by fitting Eq. (A2) to test data reported for various polymeric materials.[16–19] Figure 11 shows a plot of the octahedral shear stress (normalized by the uniaxial yield stress in tension) as a function of the normalized hydrostatic stress for several polymers: polyvinyl chloride (PVC), polystyrene (PS), polycarbonate (PC), and polymethyle methacrylate (PMMA). A linear regression analysis was performed using Eq. (A2) to fit this data. The constants a_1 and a_2 were found to be 1.908 and 0.298, respectively. The resulting equation is shown in Fig. 11 as a solid line. If the hydrostatic component had no effect on yielding, the line would be horizontal. The negative slope shows that tensile hydrostatic stresses tend to reduce the octahedral stress corresponding to yielding. Equation (A2) reduces to Eq. (A1) for the uniaxial case. Equation (A2) was used to study the effect of hydrostatic stress on yielding in the DCB specimen.

Acknowledgment

This work was performed under NASA Contact NAS1-18256.

References

[1]Wang, S. S., Mandell, J. F., and McGarry, F. J., "An Analysis of the Crack Tip Stress Field in DCB Adhesive Fracture Specimens," *International Journal of Fracture*, Vol. 14, No. 1, Feb. 1978, pp. 39–58.

[2]Crews, J. H., Jr., Shivakumar, K. N., and Raju, I. S., "Factors Influencing Elastic Stresses in Double Cantilever Beam Specimens," *Adhesive Bonded Joints: Testing, Analysis, and Design*, edited by W. S. Johnson, American Society for Testing and Materials, Philadelphia, PA, 1988, ASTM STP 981, pp. 119–132.

[3]Bucknall, C. B., *Toughened Composites*, Applied Science, London, 1977.

[4]Shivakumar, K. N. and Crews, J. H., Jr., "Bolt Clampup Relaxation in a Graphite/Epoxy Laminate," *Long-Term Behavior of Composites* (ASTM STP 813), edited by T. K. O'Brien, American Society of Testing and Materials, Philadelphia, PA, 1983, pp. 5–22.

[5]Barsoum, R. S., "On the Use of Isoparametric Finite Elements in Linear Fracture Mechanics," *International Journal for Numerical Methods in Engineering*, Vol. 10, No. 1, 1976, pp. 25–37.

[6]Hibbit, H. D., "Some Properties of Singular Isoparametric Elements," *International Journal for Numerical Methods in Engineering*, Vol. 11, No. 1, 1977, pp. 180–184.

[7]Raju, I. S. and Newman, J. C., Jr., "Methods for Analysis of Cracks in Three-Dimensional Solids," *Journal of the Aeronautical Society of India*, Vol. 36, No. 3, Aug. 1984, pp. 153–172.

[8]Freese, C. E. and Tracey, D. M., "The Natural Isoparametric Element Triangle versus Collapsed Quadrilateral for Elastic Crack Analysis," *International Journal of Fracture*, Vol. 12, No. 5, Oct. 1976, pp. 767–770.

[9]Rybicki, E. F. and Kanninen, M. F., "A Finite Element Calculation of Stress Intensity Factors by Modified Crack Closure Integral," *Engineering Fracture Mechanics*, Vol. 9, No. 4, 1977, pp. 931–938.

[10]Raju, I. S., "Calculation of Strain-Energy Release Rates with Higher Order and Singular Finite Elements," *Engineering Fracture Mechanics*, Vol. 28. No. 3, 1987, pp. 251–274.

[11]Hartranft, R. J. and Sih, G. C., "An Approximate Three-Dimensional Theory of Plates with Application to Crack Problems," *International Journal of Engineering Science*, Vol. 8, Aug. 1970, pp. 711–729.

[12]Benthem, J. P., "State of Stress at the Vertex of a Quarter-Infinite Crack in a Half-Space," *International Journal of Solids and Structures*, Vol. 13, No. 8, 1977, pp. 479–492.

[13]Raju, I. S. and Newman, J. C., Jr., "Three-Dimensional Finite Element Analysis of Finite-Thickness Fracture Specimens," NASA TN D-8414, May 1977.

[14]Atluri, S. N., Kathiresan, K., and Kobayashi, A. S., "Three-Dimensional Linear Elastic Fracture Mechanics Analysis by a Displacement Hybrid Finite Element Model," *Transactions of the 3rd International Conference on Structural Mechanics in Reactor Technology*, Paper No. L-7/3, North Holland, Berlin, 1975, pp. 1–13.

[15]Solecki, J. S. and Swedlow, J. L., "On the Three-Dimensional Implications of LEFM: Finite-Element Analysis of Straight and Curved Through Cracks in a Plate," American Society for Testing and Materials, Philadelphia, PA, ASTM STP-868, 1985, pp. 535–553.

[16]Whitney, W. and Andrews, R. D., "Yielding of Glassy Polymers: Volume Effects," *Journal of Polymer Science*, Pt. C, Vol. 16, 1967, pp. 2981–2990.

[17]Sternstein, S. S. and Ongchin, L., "Yield Criteria for Plastic Deformation of Glassy High Polymers in General Stress Fields," *American Chemical Society, Div. of Polymer Chemistry, Polymer Preprints*, Vol. 10, No. 2, Sept. 1969, pp. 1117–1124.

[18]Raghava, R., Coddell, R. M., and Yeh, G. S., "The Macroscopic Yield Behavior of Polymers," *Journal of Material Science*, Vol. 8, Feb. 1973, pp. 225–232.

[19]Carapellucci, L. M. and Yee, A. F., "The Biaxial Deformation and Yield Behavior of Bisphenol-A Polycarbonate: Effect of Anisotropy," *Polymer Engineering Science*, Vol. 26, No. 13, July 1986, pp. 920–930.

[20]Broek, D., *Elementary Engineering Fracture Mechanics*, 3rd ed., Martinus Nijhoff, Boston, MA. 1982, Chap. 4.